Association Aéronautique et Astronautique de France

57th 3AF International Conference on Applied Aerodynamics
29 - 31 March 2023, Bordeaux – France

AERO2023-54-NISHITA

UNSTEADY DSMC SIMULATION OF BLUNT NOSE WITH SPIKE AT HYPERSONIC RAREFIELD FLOWS

Nishita Ravuri[(1)], Stephen Scully[(2)] and Ashish Vashishtha[(1)]

[(1)]*Department of Aerospace & Mechanical Engineering, South East Technological University, Carlow Campus, Ireland,* *ashish.vashishtha@setu.ie*

[(2)]*Department of Electronics & Communication Engineering, South East Technological University, Carlow Campus, Ireland,*

ABSTRACT

To design an efficient ram-air intake for an air-breathing propulsion system for VLEO (Very-Low) / SLEO (Super-Low) Earth Orbit satellites requires consideration of the unsteady effects in the hypersonic low-density or rarefied environment. This study aims to analyze the unsteady effects due to shock instabilities on a forward facing spike geometry attached to a flat blunt nose in low-density hypersonic flows. The Direct Simulation Monte-Carlo (DSMC) approach is used to study two flow-conditions: 1) ground test facility (V_∞ = 2075 m/s, Kn = 1.4×10^{-3}) and 2) at an altitude of 100 km (V_∞ = 8557 m/s, Kn = 0.45) for a spiked blunt nose with flat face. It was found that gas surface interaction (specular and diffuse reflection) results in changing dynamics of flow field for both conditions. The large amplitude shock fluctuations are not observed in lower density environments as compared to continuum flow in previous literature. The diffuse reflection leads to higher drag and higher unsteadiness at V_{infty} = 2075 m/s, when compare to specular reflection, while lower drag and unsteadiness at high Knudsen number case of V_{infty} = 8557 m/s.

1. INTRODUCTION

With the advancements of space technologies in the past decades, low earth orbits (LEO, approximately above 400 km to 1000 km) have been reaching saturation point due to accumulation of man-made space debris [14] However, the LEOs have advantages of providing low or negligible drag on spacecraft, leading to their longer orbital life. But higher distance from Earth, saturation of LEOs and avoiding accumulation of future space junk, causes new interest of different space agencies (ESA/NASA/JAXA) and enterprises to develop technologies and satellites for very low earth orbits (VLEO, below 400 km) and super low earth orbits (SLEO, below 200 km). These earth orbits have the advantages of low-cost launches and provide accurate resolution for different Earth observation applications for example weather forecasting, agricultural monitoring, ocean monitoring, communication, mapping, positioning, navigation, disaster monitoring etc. However, the design of such satellites is challenging due to increased aerodynamic drag, which leads to shorter lifespans, and requires periodically orbit adjustment via the on-board propulsion system. This disadvantage can be mitigated by providing air-breathing in-space propulsion, which can accumulate the available atmospheric air for propulsion, additionally can be used to design an end-of-life re-entry burn. Some recent advancements have been made by ESA [3, 6] through the RAM-EP concept and DISCOVERER project , and by JAXA [9] via the Tsubame spacecraft.

The aerodynamic design of air-breathing satellites in VLEO/SLEO faces two competing challenges: breathing an adequate amount of air from the atmosphere for propulsion, as well as reducing aerodynamic drag to increase longer lifespans. A large cross-section intake is required to increase the collection of air for the propulsion system, which in turn leads to a penalty in drag. Hence, the design of VLEO/SLEO satellites requires careful aerodynamic consideration in hypersonic low-density or rarefied environments. Additionally, the ram-air intake in a rarefied flow regime may also experience unsteadiness due to positioning of compression front as well as gas surface interaction. In continuum regime, different blunt nose shape configurations are subjected to different degrees of unsteadiness. The spike blunt nose exhibits small amplitude, high frequency shock oscillations

[4] and high amplitude, low frequency, non-stationary pulsation [21, 5, 17] in different supersonic and hypersonic flow fields. In a similar manner, frontal hemispherical cavity in hypersonic flows are observed exhibiting small amplitude shock oscillation, which can transition to non-stationary non-linear high amplitude pulsations. [16, 19, 18, 20]. The forward injection of air - jet (or different gases) [10, 7] can also be subjected to pulsations and oscillation at different jet injection momentum.

The continuum and local thermodynamics equilibrium hypothesis is not valid in low-density flows in VLEO/SLEO orbits, due to higher free mean path (λ) between the gas molecules than characteristic length (L) of the geometry. The ratio of both can be defined as Knudsen number, ($Kn = \lambda/L$) [2]. For Knudsen number $Kn > 0.01$, the continuum hypothesis starts to breakdown, the flow can be defined as slip-stream flow ($0.01 < Kn < 0.1$), and further transitional flow can be defined between ($0.1 < Kn < 10$) and free-molecular flow zone beyond ($Kn > 10$). The aerodynamics of a non-continuum flow regime in rarefied flow can be modelled using a stochastic approach with Direct Simulation Monte Carlo (DSMC) method [1]. Among various methods for aerodynamic assessment in low-density flows (panel method, ray-tracing method, Test Particle Monte Carlo, DSMC), DSMC can provide accurate assessment of aerodynamic forces and heat transfer for different complex geometries, but requiring high computing power. With different approaches to averaging, the steady or time-varying macroscopic properties can also be computed using DSMC method. In low density environment, the aerodynamic forces will be highly dependent on gas particle interaction with the surface geometry. Based on the gas particle and surface interaction, the resultant momentum and energy is transferred to the surface, which determines the drag and heat flux on the surface. The gas surface interaction can be modelled as specular reflection and diffuse reflection as shown in Fig. 1. In specular reflection the gas particle reflects at the same angle as incident angle after interaction with surface, yielding only normal momentum exchange. The reflected velocity will depends on amount of energy exchange to the surface. In diffuse reflection, the gas particle reflect through the probabilistic velocity and direction distribution. The degree of specular and diffuse reflection is modelled with accommodation coefficient ($0 < \alpha < 1$), which depends on surface properties, orientation and gas environment. VLEO has Atomic Oxygen as dominant component, which can cause degradation of surface, and may be subjected to diffuse reflections. The frontal geometries (normal to flow direction) are subjected to higher momentum exchange in specular reflection than diffuse reflection. However, in geometries oriented non-normal to flow direction, the opposite may be true [8]. This study is motivated to explore design approaches for ram-air intake assisted with compression by spike-geometry without higher pressure losses. It aims to simulate the unsteady aerodynamic effects for a well known spike configuration with frontal base, before designing the compression assisted ram-air intake for low-density flows. The two velocity configurations are simulated using two-dimensional axisymmetric DSMC modelling: approximately 60 km altitude and 100 km altitude, both with Nitrogen as the test gas. The effects of accommodation coefficients to model specular and diffuse reflection are also studied for both cases.

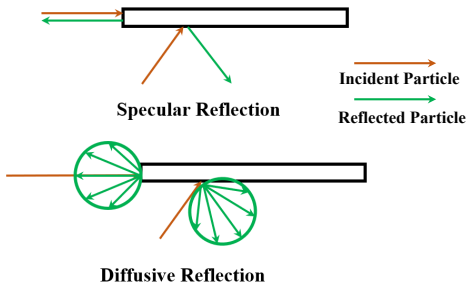

Figure 1: Gas Surface Interaction: Specular Reflection (Top), Diffuse Reflection (Bottom).

2. NUMERICAL METHOD

The open-source DSMC Solver SPARTA (**S**tochastic **PA**rallel **R**arefied-gas **T**ime-accurate Analyser) [15] is used to simulate hypersonic time-dependent cases of a spiked-blunt geometry in the low density environments. SPARTA has been validated for various rarefied flow conditions in similar velocity regime as simulated in current case [11].

2.1 DSMC Technique

Non-continuum flows are mainly characterised by two conditions: 1) the mean-free path being larger than the characteristic size of the gas flow, 2) the mean-free time is larger than or close to the time interval between a significant change in macroscopic variables. Therefore, macroscopic variables (pressure, total temperature in flow-field) cannot be tracked under the above conditions without considering more terms in the kinetic equation. The DSMC technique is a stochastic numerical method that solves the Boltzmann Equation for dilute gas flows. It aims to solve two terms, the collisionless advection and the inter-molecular collision term. A general form of the equation is as follows:

$$\frac{\partial f}{\partial t} + \boldsymbol{v} \cdot \nabla_r f + F.\nabla_v f = \left[\frac{\partial f}{\partial t}\right]_{coll} \quad (1)$$

In this study, the molecular collisions are modelled with Variable Soft Sphere model (VSS) for nitrogen stream.

The surface collision is controlled with accommodation coefficient: 0 for specular collision and 0.95 for (95 %) diffuse collision, along with specified wall temperature of the body.

2.2 Computational Domain

The spike geometry with a base diameter of 250 mm is simulated by using DSMC with two-dimensional axisymmetric boundary conditions. The computational domain as well as boundary conditions are shown in Fig. 2a. The flat base of diameter (D = 250 mm) with spike of diameter ($d = 0.2D$) has been generated for different lengths $L/D = 0.5, 1.0, 1.5$ and 2.0. The overall computational domain is $3.5D \times 2D$, with inlet boundary at left injecting the particle parcels and right boundary as the outlet. The spike and base geometry was superimposed on uniform grid (175×100) utilized in the simulation. The computation grid is selected based on several simulations of different grid sizes, ratio of simulated to real particles and time-steps with available computational resources. Figure 2b shows the uniform grid for $L/D = 1$.

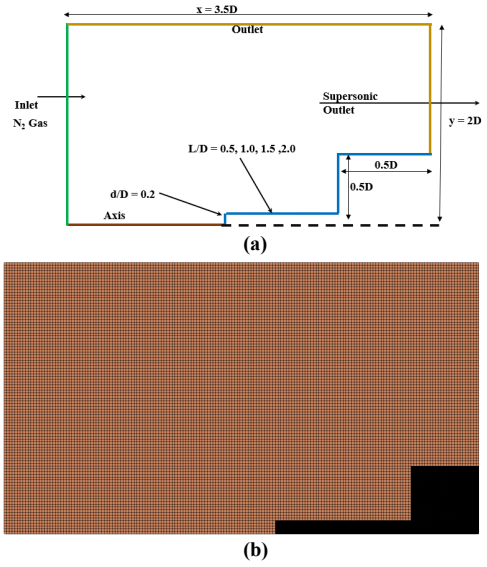

Figure 2: (a) Computational Domain, (b) Grid: $L/D = 1$

Two different flow conditions with Nitrogen as medium were simulated: 1)60 km altitude: with free stream velocity 2075 m/s, according ground testing facility LENS I [13], and 2) 100 km altitude: with free stream velocity 8557 m/s [12]. Tables 1 and 2 show the parameters used for simulations. The time-dependent unsteady simulations are completed for 2 ms total time with a constant time-step of 1×10^{-8} s. The macroscopic parameters are ensemble averaged after each 100 iterations and data has been saved for each 1×10^{-6} s. The drag coefficient was computed with momentum exchange between particle parcels and surface in axial direction. The surface pressure and total energy flux for surface elements were computed every 1 μs.

Parameters	Values
Mach Number	15.6
Free stream Density (ρ_∞)	1.763×10^{-4} kg/m^3
Free stream number Density (n_∞)	3.79×10^{21}
Free stream Temperature (T_∞)	42.6 K
Free stream Velocity (V_∞)	2075 m/s
Wall Temperature (T_w)	297 K
Gas	N_2
Mean free path (λ_∞)	0.358 mm

Table 1: Free Stream conditions for LENS facility[13]

Parameters	Values
Mach Number	30
Free stream Density (ρ_∞)	5.583×10^{-7} kg/m^3
Free stream number Density (n_∞)	1.20×10^{18}
Free stream Temperature (T_∞)	194 K
Free stream Velocity (V_∞)	8557 m/s
Wall Temperature (T_w)	297 K
Gas	N_2
Mean free path (λ_∞)	113 mm

Table 2: Free Stream conditions according to altitude 100 km [12]

3. RESULTS AND DISCUSSIONS

In continuum hypersonic flow [21, 5, 4, 17], the spiked blunt nose shows two kinds of bow-shock fluctuations: large amplitude shock pulsations and small amplitude shock oscillations. The spiked geometry in hypersonic flow was analysed as a passive drag reduction device, however, these shock fluctuations also produce unsteady drag, lift and side forces on the base body and make the flow-field unstable. The mechanism of these large pulsations and traverse oscillations is understood by many researchers consisting of cycles of ”inflation”, ”withhold” and ”collapse” in the spike and base body region [5, 4]. The flow accumulates with large vortices between the spike-surface and base-body during inflation, the pressure build-up in ”withhold” for certain time and causes sudden collapse or mass ejection near the corner of flat base. These fluctuations are mainly observed in flat base and spike geometries. The base’s curved corner [17] bleeds the mass downstream, aiding the flow stabilization and resulting no fluctuations. The ram compression in the presence of wedge or spiked body has also been considered for supersonic air-intakes for propulsion systems by establishing the oblique shock, which can compress the incoming air with reduced pressure loss than compared to

a blunt intake geometry without the wedge. With motivation to use ram-compression for air-breathing propulsion and understand the flow around a spiked blunt nose in low-density hypersonic flows, the current study simulates the spiked blunt nose with a flat base at two low-density flow conditions by using 2D axisymmetric DSMC modelling. The drag coefficients over time are presented as simulation results, incorporating effects of specular and diffuse surface reflections. Effects on wall pressure and heat flux are also discussed in subsection 3.3 for different spike lengths.

3.1 Effect on Drag Coefficient

The drag coefficients of spiked blunt nose geometries have been computed for two free stream velocity conditions (Tables 1, 2) and the time history of the same is shown in Fig. 3a and 3b, which also compares the specular and diffuse reflection effects on drag coefficients.

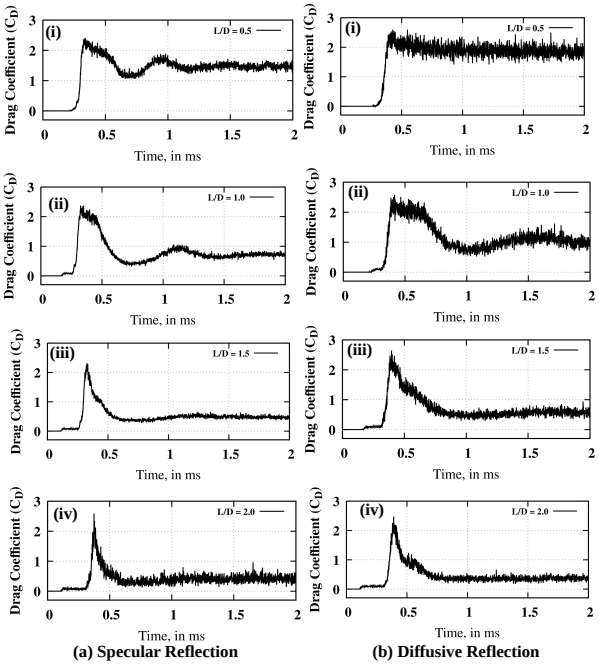

Figure 3: Time history of Drag Coefficients with (a) Specular (b) Diffuse Reflections at free stream velocity V_∞ = 2075 m/s

Figure 3 shows the time history of drag coefficient for lower altitude velocity, V_∞ = 2075 m/s with specular and diffuse reflections and spike lengths of $L/D = 0.5$, 1.0, 1.5 and 2.0. All cases show initial fluctuations in drag coefficients up to 1 ms, and settling over the next 1 ms. There are no high-amplitude fluctuations as observed in continuum cases in various literatures. In the specular reflection case, the drag coefficient fluctuations are lower than diffuse reflection, except L/D = 1.5 case. The time-

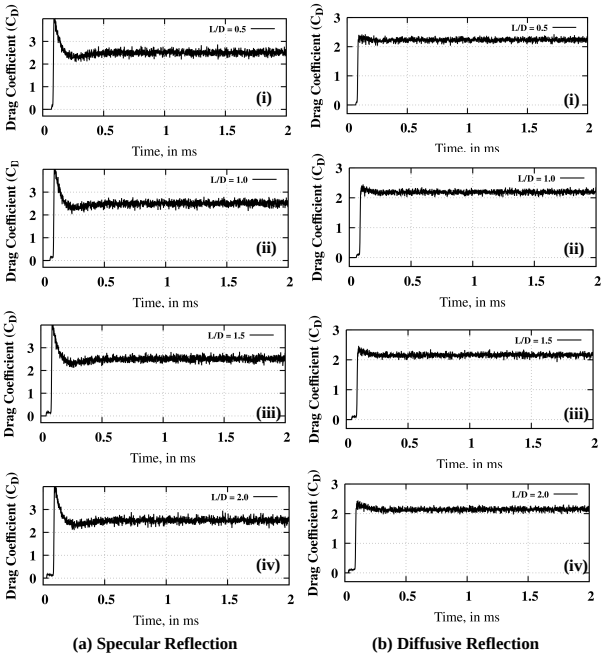

Figure 4: Time history of Drag Coefficients with (a) Specular (b) Diffuse Reflections at free stream velocity $V_\infty = 8557 m/s$

L/D	V_∞ = 2075 m/s	V_∞ = 8557 m/s
0.5 (S)	1.465 ± 0.090	2.502 ± 0.099
1.0 (S)	0.738 ± 0.098	2.506 ± 0.103
1.5 (S)	0.489 ± 0.045	2.515 ± 0.101
2.0 (S)	0.412 ± 0.107	2.526 ± 0.103
0.5 (D)	1.865 ± 0.162	2.232 ± 0.056
1.0 (D)	1.003 ± 0.181	2.190 ± 0.055
1.5 (D)	0.543 ± 0.097	2.161 ± 0.057
2.0 (D)	0.357 ± 0.068	2.143 ± 0.056

Table 3: Time-averaged (for t = 1ms to 2 ms) Drag Coefficient $\pm$ Standard Deviation, S: Specular Reflection & D: Diffuse Reflection

averaged drag coefficient between 1 ms and 2 ms along with standard deviation are tabulated for different cases in Table 3. With increasing spike length, the drag coefficient decreases up to 72 % in the case of L/D = 2.0 in specular reflection, while decreases up to 80 % in diffuse reflection cases. The diffuse reflection shows a higher drag coefficient for incoming velocity $V_\infty = 2075$ m/s, except L/D = 2.0 case. The standard deviation (measure of dispersion around the mean) in the duration of time-averaged drag coefficient remains smaller in the specular reflection case, except L/D = 2.0 in comparison to diffuse reflection case. The time history of drag coefficient at lower density environment and V_∞ = 8557 m/s is plotted for specular and diffuse reflection in Figure 4. The drag coefficient at lower density environment shows lower fluctuations in case of diffuse reflection than the specular reflec-

tion cases. The time-averaged drag coefficient (as tabulated in Table 3) for lower density environments is always higher when compared to higher density environment for V_∞ = 2075 m/s for both specular and diffuse reflection cases. Between specular and diffuse reflection, the time-averaged drag coefficient is always lower for diffuse reflection. The time-averaged drag coefficient remains constant or increases minutely up to 1% with increase in spike length for specular reflection cases at lower density. However, it decreases up to 4 % in diffuse reflection case with increase in spike length. The standard deviation or fluctuations in drag coefficient around mean is also lower in diffuse reflection case, which compared to individual specular reflection cases for different spike length.

3.2 Flow field Analysis

The flow field around the spiked blunt nose are shown in Figures 5 and 6 for different spike lengths at free stream velocities V_∞ = 2075 and 8557 m/s by plotting pressure countors.

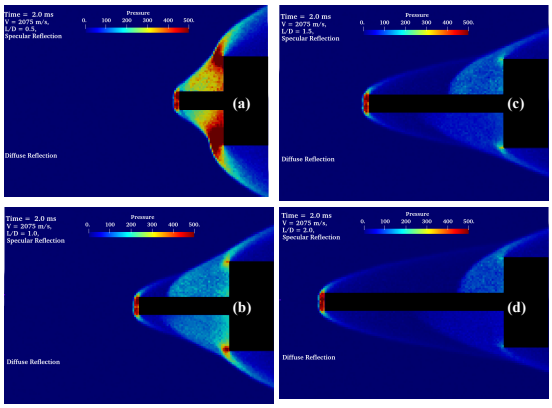

Figure 5: Flow field for specular (top half), and diffuse (bottom half) reflection (a) L/D = 0.5, (b) L/D = 1.0, (c) L/D = 1.5 and (d) L/D = 2.0, at free stream velocity V_∞ = 2075 m/s

At V_∞ = 2075 m/s, the flow field shows a bow shock near the spike tip, which interacts with the base body bow shock near the top corner. With increase in spike length (L/D), the shock interaction pattern near the top corner changes, which vary pressure distribution on the base body. The specular and diffuse reflection also changes the pressure distribution in the region between spike and base body. At longer spike length three distinct compression regions are observed at 1) spike tip, 2) frontal base, 3) compressed region between spike lateral and front base. While comparing specular (top half image) and diffuse reflection (bottom half image) for L/D = 0.5 (Fig. 5a), it can be seen that the bow-shock curvature altered between specular and diffuse reflection. The front shock became inward curved in diffuse reflection and interacts with base bow shock inner of the top base corner in comparison to specular reflection, which results in a larger high pressure region. Similar effects are observed for L/D = 1.0, 1.5 and 2.0 (Fig. 5 b,c and d), where the high pressure region attached to front base body become distributed between base and spike surface region. The distributed pressure between front base and lateral spike surface may introduce lower unsteadiness in diffuse reflection than in specular reflection at V_∞ = 2075 m/s. At

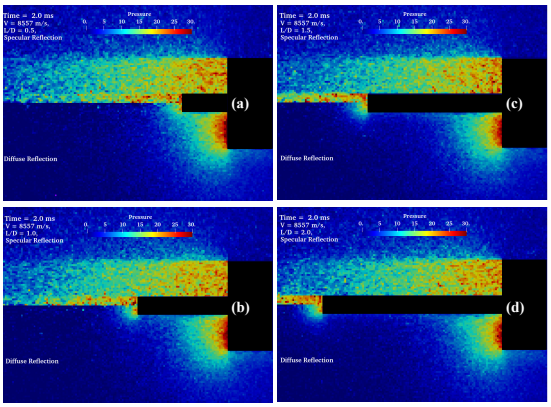

Figure 6: Flow field for specular (top half), and diffuse (bottom half) reflection (a) L/D = 0.5, (b) L/D = 1.0, (c) L/D = 1.5 and (d) L/D = 2.0, at free stream velocity V_∞ = 8557 m/s

V_∞ = 8557 m/s, lower density environment, the effect of specular and diffuse reflection on flow-field is more distinct as shown in Fig. 6. The overall maximum pressure is lower in this case, when compared to V_∞ = 2075 m/s, but specular reflection at lower density leads to perfect reflection of molecules to larger upstream distances from flat base and flat spike face in comparison to diffuse reflection. In Fig. 6 all specular reflection cases show larger extent of gas molecule reflections with little effect of spike length, while diffuse reflection shows high pressure regions at spike tip and frontal base accordingly. With an increase in spike length, the high pressure region in specular reflection increases slightly which explains the overall hike in drag coefficient values for the specular reflection case in column 2 of Table 3. In the case of diffuse reflection, increase in spike length separates the high pressure regions of spike tip and frontal base, leading up to 4 % reduction in overall drag coefficient values (Column 2 of 3). The flow-field analysis also suggests that diffuse reflection surfaces with compact pressure region may introduce lower unsteadiness in comparison to specular reflection at a lower density environment.

3.3 Effect on Wall Pressure and Heat Flux

The time averaged (between 1 - 2 ms) wall pressure along the surface length for specular and diffuse reflection for

all the spike lengths are plotted in Fig. 7 for both the free stream velocities. The first peak in all the plots represents the high pressure at spike tip and the second peak shows the pressure variation at flat base surface. At free stream velocity V_∞ = 2075 m/s and L/D = 0.5, 1.0 the spike lateral surface shows higher pressure with an additional peak in specular and diffuse reflection (Fig. 7), which reduces in L/D = 1.5 and 2.0. This additional peak is due to spike and base surface shock interaction and high compression region between spike and frontal base. The specular reflection shows lower total wall pressure (area under the curve) for all spike lengths in comparison to diffuse reflection at free stream velocity V_∞ = 2075 m/s, which leads to lower drag in specular reflection than compared to diffuse reflection. In the specular reflection case

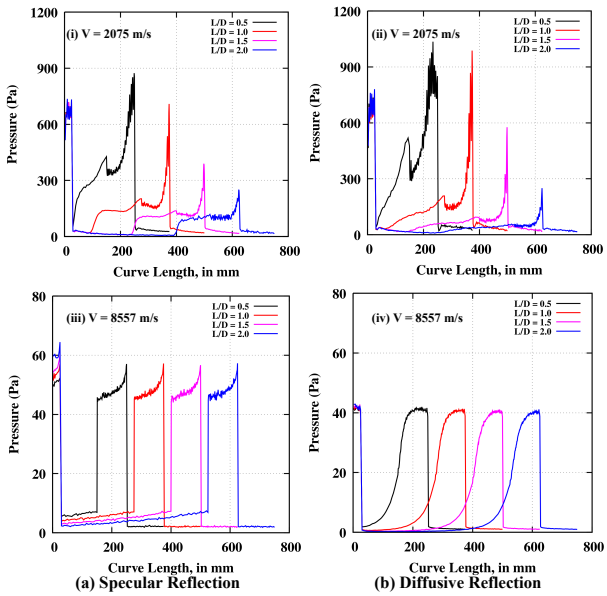

Figure 7: Time-averaged (t = 1.0 - 2.0 ms) Wall Pressure for (a) Specular & (b) Diffuse Reflection

at lower density environment and free stream speed V_∞ = 8557 m/s, the gas molecules interact separately at the spike tip and frontal base, shows the sudden peaks in wall pressure for all the spike lengths with almost same magnitude. In diffuse reflection at V_∞ = 8557 m/s, gradual pressure increase at spike lateral surface along with smooth lower peak at frontal base as shown in Fig. 7 b(iv). In lower density environments, specular reflection leads to relatively higher total wall pressure in comparison to diffuse reflection. The compression regions are well separated at V_∞ = 8557 m/s compared to V_∞ = 2075 m/s. However, the diffuse reflection contributes to a higher wall pressure on lateral surfaces of geometry, but lower pressure at frontal surfaces (spike tip and frontal base body). The time averaged (between 1 - 2 ms) wall heat flux along surface length is compared between diffuse reflection between free stream velocities V_∞ = 2075 m/s and V_∞ = 8557

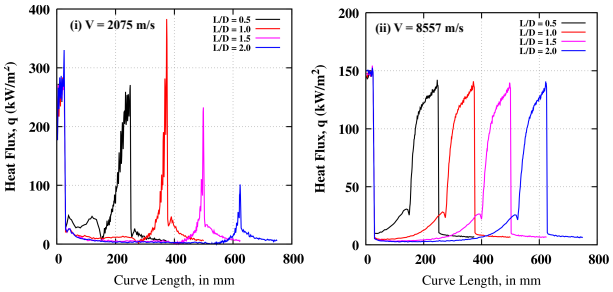

Figure 8: Time-averaged (t = 1.0 - 2.0 ms) Wall Heat Flux at (i) 2075 m/s (ii) 8557 m/s for Diffuse Reflection

m/s cases in Fig. 8. The wall heat flux distribution is affected by spike length at V_∞ = 2075 m/s and there is no effect of spike length (Fig. 8 ii) at lower density environment at free stream velocity V_∞ = 8557 m/s. The second peak in wall heat flux plots represents the wall heat flux at frontal base. At L/D = 0.5 and 1.0, the wall heat flux is higher due to interaction between spike shock and base compression region, while higher spike length L/D = 1.5 and 2.0 shows reduced wall heat flux by moving the interaction point away from the frontal surface. The wall heat flux reduces for L/D = 2.0 than compared to L/D = 1.5, due to longer relaxation region between spike tip and frontal base. At the lower density with free stream velocity V_∞ = 8557 m/s, all the spike lengths do not affect the wall heat flux on the surface due to separated compression regions.

4. CONCLUSIONS

In non-continuum hypersonic flows, the spike geometry with frontal base does not show large amplitude flow fluctuations as reported in the literature [5, 4, 17] for continumm high density flow fields at hypersonic speeds. However, small amplitude fluctuations are found during time-history analysis of drag coefficient of spike geometry, which is affected by the gas surface interactions at the two simulated free stream conditions, corresponding to the altitudes of 60 km (V_∞ = 2075 m/s) and 100 km (V_∞ = 8557 m/s). The specular reflection contributed to a lower time averaged drag coefficient than compared to diffuse reflection at free stream velocity V_∞ = 2075 m/s. At higher altitude conditions, diffuse reflection showed lower drag-coefficient than for that of specular reflection. The spike length reduces the drag coefficients at 60 km altitude conditions significantly for both specular and diffuse reflection. At higher altitude (100 km) condition, with increase in spike length, the drag coefficient remains almost constant with specular reflection, but reduces sightly with diffuse reflection. At higher altitude, the wall heat flux for diffuse reflection does not change with spike length, but reduces at 60 km altitude with increase in spike length.

ACKNOWLEDGMENT

The authors wish to acknowledge Irish Research Council Postgraduate Scholarship (under grant number GOIPG/2022/1832) for providing the financial support to carry out current research.

REFERENCES

[1] GA Bird. Direct simulation and the boltzmann equation. *The Physics of Fluids*, 13(11):2676–2681, 1970.

[2] Graeme A Bird. Molecular gas dynamics and the direct simulation of gas flows. *Molecular gas dynamics and the direct simulation of gas flows*, 1994.

[3] E. Ferrato, V. Giannetti, A. Piragino, M. Andrenucci, T. Andreussi, and C.A. Paissoni. Development roadmap of sitael's ram-ep system. In *Proceedings of* 36^{th} *International Electric Propulsion Conference, University of Vienna, Austria, IEPC-2019-886*, 2019.

[4] D. Feszty, K. J. Badcock, and B. E. Richards. Driving mechanisms of high-speed unsteady spiked body flows, part i: Pulsation mode. *AIAA Journal*, 42(1):95–106, 2004.

[5] D. Feszty, B. E. Richards, K. J. Badcock, and M. A. Woodgate. Numerical simulation of a pulsating flow arising over an axisymmetric spiked blunt body at Mach 2.21 and Mach 6.00. *Shock Waves*, 10:323–331, 2000.

[6] S.J. Haigh, R.E. Lyons, V.T.A. Oiko, A.M.A. Rojas, K.L. Smith, J. Becedas, G. González, I. Vázquez, Á. Braña, K. Antonini, K. Bay, L. Ghizoni, V. Jungnell, J. Morsbøl, T. Binder, A. Boxberger, G.H. Herdrich, F. Romano, S. Fasoulas, D. Garcia-Almiñana, S. Rodriguez-Donaire, D. Kataria, M. Davidson, R. Outlaw, B. Belkouchi, A. Conte, J.S. Perez, R. Villain, B. Heißerer, and A. Schwalber. Discoverer - radical redesign of earth observation satellites for sustained operation at significantly lower altitudes. In *Proceedings of the 68th International Astronautical Congress (IAC 2017)*, pages 9254–9262, 2017.

[7] P. Harmon, A. Vashishtha, D. Callaghan, C. Nolan, and R. Deiterding. Study of direct gas injection into stagnation zone of blunt nose at hypersonic flow. In *AIAA Propulsion & Energy Forum*. AIAA 2021-3529, 2021.

[8] F. Hild, C. Traub, M. Pfeiffer, J. Beyer, and S. Fasoulas. Optimisation of satellite geometries in very low earth orbits for drag minimisation and lifetime extension. *Acta Astronautica*, 201:340–352, 2022.

[9] Y. Hisamoto, Kazutaka Nishiyama, and H. Kuninaka. Design of air intake for air breathing ion engine. *Proceedings of the International Astronautical Congress, IAC*, 9:7630–7634, 01 2012.

[10] J. W. Keyes and J. N. Hefner. Effect of forward-facing jets on aerodynamic characteristics of blunt configurations at mach 6. *Journal of Spacecraft and Rockets*, 4(4):533–534, 1967.

[11] A. G. Klothakis, I. K. Nikolos, T. P. Koehler, M. A. Gallis, and S. J. Plimpton. Validation simulations of the dsmc code sparta. *AIP Conference Proceedings*, 1786(1):050016, 2016.

[12] J. Moss. *DSMC Simulations of Ballute Aerothermodynamics Under Hypersonic Rarefied Conditions*.

[13] J. Moss and G. Bird. *DSMC Simulations of Hypersonic Flows with Shock Interactions and Validation with Experiments*.

[14] C Pardini and L. Anselmo. Evaluating the impact of space activities in low earth orbit. *Acta Astronautica*, 184:11–22, 2021.

[15] S. J. Plimpton, S. G. Moore, A. Borner, A. K. Stagg, T. P. Koehler, J. R. Torczynski, and M. A. Gallis. Direct simulation monte carlo on petaflop supercomputers and beyond. *Physics of Fluids*, 31(8):086101, 2019.

[16] A. Vashishtha. *Bow-Shock Instability and its Control in front of Concave shaped Blunt Nose at Hypersonic Mach No. 7*. PhD thesis, Department of Advanced Energy, 2016.

[17] A. Vashishtha and S. Khurana. Pulsating flow investigation for spiked blunt-nose body in hypersonic flow and its control. In *AIAA Scitech 2021 Forum*. AIAA 2021-0839, 2021.

[18] A. Vashishtha, Y. Watanabe, and Suzuki K. Study of bow-shock instabilities in front of hemispherical shell at hypersonic Mach number 7. In *45th AIAA Fluid Dynamics Conference*. AIAA 2015-2638, 2015.

[19] A. Vashishtha, Y. Watanabe, and Suzuki K. Study of shock shape in front of concave, convex and flat arc in hypersonic flow. *JAXA-SP-14-010*, pages 127–132, mar 2015.

[20] A. Vashishtha, Y. Watanabe, and Suzuki K. Bow-shock instability and its control in front of hemispherical concave shell at hypersonic Mach number 7. *Transaction of the JSASS, Aerospace Technology Japan*, 14(ists30):121–128, 2016.

[21] C. J. Wood. Hypersonic flow over spiked cones. *Journal of Fluid Mechanics*, 12, 1961.